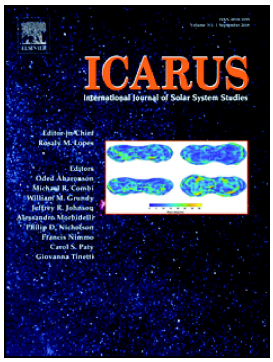

Temporal variation of the 3-micron hydrocarbon emissions at the 8-micron north polar hot spot of Jupiter: Comparison with solar wind activity

Sang Joon Kim, Chae Kyung Sim, Thomas R. Geballe, Yuk L. Yung, Steve Miller, Thomas K. Greathouse, Sungho Lee, Chihiro Tao

PII: S0019-1035(20)30233-5

DOI: https://doi.org/10.1016/j.icarus.2020.113852

Reference: YICAR 113852

To appear in: *Icarus*

Received date: 25 July 2019

Revised date: 3 April 2020

Accepted date: 11 May 2020

Please cite this article as: S.J. Kim, C.K. Sim, T.R. Geballe, et al., Temporal variation of the 3-micron hydrocarbon emissions at the 8-micron north polar hot spot of Jupiter: Comparison with solar wind activity, *Icarus* (2020), https://doi.org/10.1016/j.icarus.2020.113852

Temporal Variation of the 3-micron Hydrocarbon Emissions at the 8-micron North Polar Hot Spot of Jupiter: Comparison with Solar Wind Activity

Sang Joon Kim[a,*], Chae Kyung Sim[a], Thomas R. Geballe[b], Yuk L. Yung[c], Steve Miller[d], Thomas K. Greathouse[e], Sungho Lee[f] and Chihiro Tao[g]

[a]School of Space Research, Kyung Hee University, Yongin, 446-701 Korea

[b]Gemini Observatory, 670 N. A'ohoku Place, Hilo, HI 96720 USA

[c]Division of Geological and Planetary Sciences, Caltech, Pasadena, CA 91125 USA

[d]Department of Physics and Astronomy, University College London, London WC1E 6BT, U.K.

[e]Southwest Research Institute, 6220 Culebra Road, San Antonio, TX 78238, USA

[f]Korea Astronomy and Space Science Institute (KASI), Daejeon, 305-348 Korea

[g]Institute of Space and Astronautical Science, Japan Aerospace Exploration Agency, Japan.

Submitted to Icarus on July 25, 2019. Revised on Dec. 31, 2019; April 4, 2020.

Running title: Variations of 3-μm Hydrocarbon Emissions on the 8-μm North Polar Hot Spot of Jupiter

Keywords: Jupiter, Infrared, Spectroscopy, Atmosphere, Aurora

*Editorial correspondence and proofs should be directed to:

Sang Joon Kim

School of Space Research, Kyunghee University, Yongin, Kyunggido, 446-701 Korea

e-mail: sjkim1@khu.ac.kr

tel: 82-10-6620-2389

Abstract

We have obtained Gemini / GNIRS 3.3 - 3.4 μm spectra of Jupiter at 65^{o} North latitude over a range of longitudes roughly centered on the 8-μm CH_4 north polar hot spot (8CNPHS). The spectra were measured on four occasions during a **four**-month period in 2018, in order to search for variability of the 3-μm emissions of CH_4 and C_2H_6. The observed locations of the brightest spots of the C_2H_6 and CH_4 emissions at 65^{o}**N** differed in longitude typically by 20 ^{o} during this period. The peak emission intensities of these species showed large variations, with the highest intensities 3-4 times greater than the lowest intensities. In addition, the brightest 3-μm CH_4 emissions and hottest temperatures at the 8CNPHS were significantly less than those at the 3-μm CH_4 north polar hot spot (3CNPHS, Kim et al. 2015). Recently, Sinclair et al. (2019) reported a coincidence betwee**n s**olar wind **dynamical pressure** and the 8-μm brightening of the 8CNPHS. In contrast, we find lack of correlation in our data between the 3-μm hydrocarbon emission intensities at the 8CNPHS and the solar wind strength. We also find lack of correlation between H_3^+ intensities and the solar wind strength during the period. However, due to the limited observational data, it is too early to conclude whether this lack of correlation indicates that the solar wind activity induced no significant changes in local temperatures (<40K) and/or mixing ratios of these molecules. Our observing period was close to the historic grand solar minimum. The detailed influence of the solar activity on the 3 and 8 μm brightness at the 8CNPHS is not quantitatively understood at the present time.

1) Introduction

Jupiter's polar regions exhibit bright aurorae in the UV and IR ranges due to particle precipitation from the jovian magnetosphere. Infrared (IR) images at 8-μm show stratospheric (p = 0.1 - 10 mbar) thermal line emission from CH_4 and regions of higher temperatures, or "hotspots," close to the magnetic North and South poles (Caldwell et al., 1980; Kim et al., 1985; Drossart et al., 1993). The 8-μm north-polar hot spot (8CNPHS) has been stationary at 180° (SysIII) longitude, +65° N latitude since the detection in early 1980s (Caldwell et al., 1980; Sinclair et al., 2019). The underlying cause(s) of the hotspots and their motion and/or lack thereof are not understood.

Investigations of another major fundamental band of CH_4 and its combination bands at 3.3-μm should be helpful in understanding the nature of the 8-μm hotspots, not only because the peak 3.3-μm and 8-μm emissions occur at μbar and mbar pressure levels, respectively (Kim et al. 2017), but also because the excitation mechanisms of different bands require different energetic processes and can reveal additional aspects of auroral activity. The morphology of the 3.3-μm CH_4 emission in the auroral region of Jupiter has been studied previously using ground-based spectro-imaging observations with the Gemini North / Gemini Near-Infrared Spectrograph (GNIRS) on 2013 January 13 and February 4 (Kim et al., 2015), and also by the space probes Galileo/Near-Infrared Mapping Spectrometer (NIMS) in 1997 September (Altieri et al., 2016) and Juno/ Jupiter InfraRed Auroral Mapper (JIRAM) in 2016 August (Moriconi et al., 2017). Kim et al. (2015) found that the brightest 3.3-μm CH_4 emission was located at SysIII longitude 197°, and thus

not coincident with the 8CNPHS. Moriconi et al. (2017) found that the 3.3-μm northern auroral CH_4 emission observed at a different time than Kim et al. (2015) was located at roughly the same longitude, ~205^o (SysIII). However, whether or not there were significant morphological differences at these times is unclear, because the ground-based GNIRS observations of the CH_4 emission from the high-latitude auroral regions are spatially limited, and the low resolution CH_4 spectra obtained by JIRAM do not separate lines of CH_4 from adjacent strong H_3^+ lines. Kim et al. (2015) also found that the temperature of the 3.3-μm CH_4 north polar bright spot (hereafter 3CNPHS) is ~500K, showing that high temperatures are present at high altitudes. In addition, Kim et al. (2017) examined the 3.3-μm and 8-μm CH_4 spectra from the 8CNPHS observed at Gemini North / GNIRS and IRTF / TEXES on 2013 Jan. 13, and 2013 Feb. 6, respectively, and found that at the μbar pressure levels of the 8CNPHS, temperatures (<350K) are lower than those at the 3CNPHS and also are lower than for the cold 8CNPHS model proposed by Drossart et al. (1993).

Jupiter's aurora is known to be less influenced by solar activities than are the aurorae of Earth and Saturn (e.g., Hill, 2001 and 2004; Cowley and Bunce, 2001). However, there have been reports of correlations between solar activity and Jupiter's UV, near-IR H_3^+ line emission and mid-IR hydrocarbon aurorae. A brightening of jovian UV polar emission was detected during increases of the solar wind dynamic pressure (Waite et al., 2001; Pryor et al., 2005; Nichols et al., 2007; Nichols et al., 2017). Kita et al. (2016) has reported a correlation between the duration of the quiescent interval of the solar wind and the auroral power, although a direct correlation of the UV auroral emission and solar wind was not readily apparent. At near-IR wavelengths, Baron et al. (1996) reported that the daily variation of the H_3^+ auroral intensity is small (<20%), but is well correlated with the variation of solar wind pressure, although a longer term correlatio**n d**uring a **four-**month period was not clear. In the mid-IR range, Kostiuk et al. (2011) found a possible correlation between the northern **12**-μm C_2H_6 emission and an index of solar activity equivalent to sunspot number based on ground-based observations since 1982 and Voyager 1 and 2 observations in 1979.

Recently, Sinclair et al. (2019) report a brightening of the 8-μm CH_4 emission at the 8CNPHS in Jan. 2017 during a period of solar wind compression. They suggest that this was due to a temperature increase at μbar pressure levels caused by the increase of solar wind dynamic press**ure. The** majority of the 8-μm emission originates from the mbar pressure level, where temperature changes due to solar wind effects are not expected. They also suggest that either a change in the abundance of CH_4 or variable non-LTE emission could explain the observed brighhtening.

This paper describes a search for monthly variations of the 3.3-μm CH_4 and C_2H_6 emissions at the 8CNPHS, which was observed four times during early - mid 2018 by GNIRS/Gemini North. Bright transient events in these emissions could be the signature of concentrations of high energy electron precipitation there, which could be correlated with solar wind activities and thus be the cause of the 8CNPHS. While the near-IR H_3^+ and the 8-μm CH_4 emissions mainly originate from nano-bar and mbar pressure levels, respectively, the 3.3-μm CH_4 and C_2H_6 emissions at the 8CNPHS mostly originate from the intermediate μbar pressure levels, where the influence of the solar wind might be manifested as suggested by Sinclair et al. (2019).

2) Observations and Data Reduction

Gemini North / GNIRS observations of the north polar region near 65^{o}**N** latitude were carried out on 2018 March 15, May 14, June 29, and July 26, (UT) for program GN-2018A-Q-221, at times when the 8CNPHS was near the central meridian longitude. The observing log is provided in Table 1. The observational configuration was the same as that of our previous GNIRS observations in 2013 (Kim et al., 2015), except that the 0.1 arcsec (2-pixel) wide, 49 arcsec long slit was oriented parallel to 65^{o}**N** latitude at the central meridian longitude (CML) rather than along the CML. The covered wavelength range was 3.315 - 3.415 μm at a spectral resolving power of ~18,000. The wavelength range includes lines of CH_4, C_2H_6, and H_3^+, which are in emission at the 8CNPHS and adjacent longitudes. Individual exposures were 140 seconds with 12 exposures per night, except 10 exposures on July 26. The telescope was nodded +/- 15 arcsec east-west between exposures, which maintained the same strip of Jupiter including the hot spot in the slit while allowing sky emission lines to be removed by subtracting pairs of spectro-images. Standard stars, HIP77811 (V=5.04, B3V) and HIP69974 (V=4.52, A1V), were observed immediately before or after Jupiter to provide intensity and wavelength calibrations of the March/May, and June/July observations, respectively. They were selected so that their airmasses closely matched those of Jupiter during the observations. Weather conditions were marginal for these observations, with intermittent thin clouds, variable seeing, and high and time-variable water vapor columns above Mauna Kea.

The absolute intensities presented in Figure 1abcd were obtained from the observed fluxes of the standard stars as well as by cross-checking the previous absolute calibrations of the 3.3-μm continuum levels of the non-auroral regions observed by UKIRT/CGS4 (Kim et al. 2010), ISO (Kim et al. 2014), and Gemini North/GNIRS (Kim et al. 2015). A discussion of the uncertainties in the intensities is given below. The seeing at 3.4 μm was typically 0.5 – 0.75 arcsec; thus, the range of latitudes sampled was considerably wider than implied by the slit width, but was much less than the latitudinal width of the hotspot, which is typically ~5 arcsec.

Table 1. Observing Log

Jupiter Observation Date and Time	Exposure Times (seconds)	Water vapor	Seeing arcsec, 3.3μm	Standard Star	Mean Airmasses (Jupiter, Standard Star)
March 15, 2018 13:15 -13:42 (UT)	12 x 140 s	>6mm	~0.50	HIP77811	1.28, 1.33
May 14, 2018 09:57 - 10:24 (UT)	12 x 140 s	1 mm	~0.75	HIP77811	1.24, 1.30
June 29, 2018 07:50 - 08:18 (UT)	12 x 140 s	4 mm	~0.65	HIP69974	1.32, 1.28
July 26, 2018 06:07 - 06:27 (UT)	10 x 140 s	5 mm	~0.75	HIP69974	1.32, 1.29

The slit was positioned at the central latitude of the 8CNPHS (65^{o} N) on Jupiter by performing a blind offset of the telescope from either a nearby star or one of the Galilean satellites. The positioning accuracy was checked by measuring the angular extent of the chord of emission from Jupiter in the spectral images. In all cases we conclude that the north-south positioning accuracy was better than one arcsecond. As the dimensions of the 8CNPHS and 3CNPHS are at least several arcseconds, we are confident that pointing errors are unimportant.

Figure 1abcd shows the reduced 3.33 - 3.36-μm spectra of Jupiter (the portion of the observed wavelength interval where the most useful jovian emission lines occur) at the location of the 8CNPHS, the observed atmospheric transmission derived from the spectra of the standard star, and model jovian spectra (discussed in the following section) on each of the four observing dates. Each of these reduced spectra is the sum of the spectra of all ~100 rows of the GNIRS detector array within **+/-2.5** arcseconds of the nominal center of the 8CNPHS at 180° (SysIII) longitude as shown in Fig. 2. The gaps in the reduced spectra are at wavelength sub-intervals where the atmospheric transmission was too low to produce reliable data. Except for May 14 the high telluric water vapor column made it difficult to observe the CH_4 lines of the ν_3, $\nu_3+\nu_4-\nu_4$, and $\nu_2+\nu_3-\nu_2$ bands between 3.315 and 3.330 μm studied previously by Kim et al. (2015; see their Fig. 2). For example, note in Fig. 1abcd that the absorption depths of the telluric CH_4 P(2) line at 3.3344 μm in the standard star spectra are approximately the same on the four dates, while the absorption depths of the H_2O lines are significantly weaker in the May spectrum than in the other three spectra.

Because of the high water vapor columns, in this work we concentrate on the roughly 500 weak CH_4 lines in the wings of the Q-branches of the previously mentioned combination bands in the 3.330 - 3.336 μm interval, where the telluric absorptions are weaker, along with individual C_2H_6 ν_7 and H_3^+ lines between 3.330 and 3.400 μm that are neither significantly blended with other molecular lines nor masked by telluric absorptions and have signal-to-noise ratios greater than 2. Individual lines of the CH_4 Q-branch combination bands are unresolved from one another, but their combined signal is readily apparent in Figs. 2 and 3.

The uncertainties in the intensity levels of individual data points in Fig. 1abcd vary with wavelength due to the wavelength dependence of the telluric transmission spectrum. Moreover, on all four nights the varying water vapor column and seeing conditions during the observing nights (Table 1) results in additional uncertainty. We conservatively estimate the 1-σ noise to be 0.00005 W m^{-2} μm^{-1} sr^{-1} at wavelengths where the atmospheric transmission is at least 80%. This is significantly greater than the noise level of ~0.00001 W m^{-2} μm^{-1} sr^{-1} estimated by the GNIRS Integration Time Calculator for stable weather conditions. The uncertainties at wavelengths of higfher telluric absorption (atmospheric transmission less than 80%) must be higher than the above 1-σ noise level. The 1-σ noise levels are approximately the same for each of the four spectra, and are about the same as the intensities of the very weak but identifiable C_2H_6 ν_7 lines in March (Fig. 1a). In order to increase the S/N ratios for the emission from CH_4 and C_2H_6, at each longitude the Q-branch intensity of the CH_4 combination bands was integrated over the 3.330-3.336-μm interval and the intensities of the cleanly detected C_2H_6 ν_7 line intensities were summed to produce the intensity profiles presented in Fig. 2.

Figure 2 shows east-west intensity profiles of CH_4, H_3^+, and C_2H_6 derived from the sums of the lines mentioned above in small (~0.3-arcsec wide) regions along the slit. Because Jupiter rotated appreciably during the observations, individual pairs of jovian spectro-images were de-rotated in longitude before summing them. We also corrected for emission angle effects when de-rotating the images. In the figure the center of horizontal axis is set to 180° SysIII longitude, the center of the 8CNPHS. During the four-month period, the apparent size of Jupiter's disk also varied. The horizontal scale of Fig. 2 is that of May 14, 2018, when Jupiter was near opposition; the profiles obtained in March, June, and July were scaled to it so that the longitudes are aligned for the different dates. Regions near the limbs where S/N ratios become insignificant have been discarded. For each molecular species, the intensity profile is normalized to a peak of 30 for the brightest of the four spectra. The absolute intensities of the strongest H_3^+ lines are much higher than those of the other species. Nevertheless, the east-west intensity profiles of the CH_4 and C_2H_6 emissions are of scientific value, as can be seen in Fig. 2.

3) Results: Time Variations and Intensity Profiles

In addition to the spectra at the 8CNPHS, Figure 1abcd contains model CH_4 spectra of the blended ν_3, $\nu_3+\nu_4-\nu_4$ and $\nu_2+\nu_3-\nu_2$ bands at the best fit temperature for each spectrum. The temperatures of the CH_4 bands range from 180 K to 220 K. These are largely local thermal temperatures because the Einstein A coefficients of the pure rotational transitions of the CH_4 bands are much less than the collisional deexcitation rates at μbar pressure levels (Kim, Geballe, and Noll, 2000). They are significantly lower than the temperatures (~500K) at the 3CNPHS (Kim et al. 2015). The relatively cool mesospheric temperatures for the 8CNPHS are consistent with the result of Kim et al. (2017). In our models, we used an equatorial mixing ratio curve for CH_4 as discussed in Sec. 4b and in Appendix 1, because we do not see significant enhancements of either temperature or intensity at the 8CNPHS.

In Fig. 2 (bottom panel), it can be seen that the H_3^+ emission peaks, near longitudes of 200^o and 150^o approximately coincide with those of the established main auroral oval, and also with the positions of those peaks observed in 2013 by Kim et al. (2015). The relative H_3^+ intensities during the four-month period varied significantly and are approximately consistent with the maximum intensity variation of a factor of 3 observed by Baron et al. (1996), except for the March 15 data, when the H_3^+ emission at 200^o was unusually weak.

Because the CH_4 intensities in Fig. 2 are derived from many weak lines, the CH_4 intensity profiles follow the behavior of the band and not that of any individual line. As shown in Fig. 2, the May and June peaks of the CH_4 emissions roughly coincide in longitude with those of H_3^+, but the widths of the CH_4 peaks are about twice those of H_3^+. We note, however, that in 2013 January the peak CH_4 line emission occurred between the H_3^+ emission peak and the 180^o SysIII longitude (Kim et al., 2015), implying that the position of the CH_4 peak has varied. In the March and July data, the CH_4 emissions are significantly lower. The brightest regions of the CH_4 emissions were roughly stationary between 2018 May 14 and June 29. In contrast, the positions of the C_2H_6 emission peaks moved from ~190^o to ~180^o SysIII longitude during the period. The locations of the C_2H_6 and CH_4 emission peaks differed in longitude typically by 20^o during this period. The possible cause or causes of the variations of the C_2H_6 and CH_4 emission peaks are not clear at the present time, as discussed in the next section.

In Fig. 3 the 3.3-μm CH_4, C_2H_6, and H_3^+ emission intensities, obtained from summing 100 spectra within the 8CNPHS marked in the top panel of Fig. 2, are plotted against time. The brightest CH_4 and C_2H_6 emissions at the 8CNPHS occurred on May 14, 2018, with the intensities 2.8 and 4.4 times, respectively, greater than those on March 15, 2018. In contrast the H_3^+ emission was brightest on June 29. Figure 3 also compares the above intensities with the solar wind dynamic pressures (nPa), derived from the solar-wind propagation model of Tao et al. (2005). The model utilizes hourly-resolved measurements of the solar-wind and magnetic field at Earth's bow-shock nose from OMNI (Thatcher et al., 2011) as input data, and extrapolates the solar-wind flow to the magnetosphere of Jupiter. The limitations of the model are described in detail in Tao et al. (2005). We set an uncertainty of ± 2 days, the horizontal bars in Fig. 3, based

on the model uncertainty at the orbit of Jupiter. The March 15 and July 26 data points coincide with medium sized solar wind bursts of 0.25~0.30 nPa within the model error bar, but the much stronger May 14 and June 29 emissions do not coincide with any significant enhancement of the solar wind dynamic pressure. We thus find lack of correlation between the 3.3-μm emission and solar wind dynamic pressures in our observations. We also find that other solar wind parameters, such as densities, radial velocities, temperatures, etc. (which are not shown here) are not correlated with the 3.3-μm emissions at the 8CNPHS. In addition, no correlations between the emission at the 3CNPHS (Kim et al. 2017) and the solar wind parameters are apparent when the same comparision methods are employed.

We also searched for correlations between the brightening of the 3-μm emissions at the 8CNPHS and the accumulations of solar wind particles during the quiescent intervals. For this, we used the same definitions of the following parameters that Kita et al. (2016) used: the duration of the quiescent interval, the variation of the solar wind dynamic pressure presented in Fig. 3, and the threshold value between the solar wind quiescent and compression period. We find no such correlation during early – mid 2018.

We note that 2018 March - July was only ~2 years before the next solar minimun in ~2020, and is possibly close to the historic grand solar minimum (e.g., Solanki and Krivova, 2011). Clearly the sun was not very active during our observing period. The effect of low solar activity on the 8CNPHS is not known at the present time.

4) Possible Causes of the Variations of the 3.3-μm CH_4 and C_2H_6 Emissions

Because there is lack of correlation between solar wind activity and the intensity variations of the line emision at the 8CNHS/3CNPHS, one or more other mechanisms must be responsible for the temporal variations of 3.3-μm CH_4 and C_2H_6 auroral emissions. In this section we discuss several possible explanations: variations in (a) temperatures, (b) CH_4 mixing ratios, and (c) auroral particle bombardment and Joule heating (Yates et al., 2014).

(4a) Temperatures at the 8CNPHS

The 3.3-μm hydrocarbon emission, which normally is due almost entirely to fluorescence and not to thermal emission, is relatively insensitive to temperature compared with the 8-μm hydrocarbon emission (Kim et al., 2014). Sinclair et al. (2018; 2019) show that an increase of ~20 K at μbar pressure levels can cause more than a factor of 2 increase in the 8-μm CH_4 emission at the 8CNPHS compared with that of quiescent north polar regions, although the majority of the 8-μm CH_4 emission originates from mbar pressure levels (Fig. S3 of Sinclair et al., 2019). In contrast, based on the T-P and CH_4 mixing ratio profiles derived by Kim et al. (2017), an increase in temperature greater than ~70 K at the μbar levels in the auroral regions is needed to produce an increase in the thermal emission at 3.3 μm that is comparable to the 1-σ uncertainty (0.0001 Wm^{-2} μm^{-1} sr^{-1}) of the 2013B spectrum in Fig. 1 of Kim et al. (2017). However, the CH_4

mixing ratio curve is highly uncertain at μbar pressures levels (e.g., Fig. S5 of Sinclair et al., 2019; Fig. 3a of Kim et al., 2017) and it is important to constrain it more tightly. We have done this, as discussed below.

(4b) Variations in CH_4 mixing ratios

In Appendix A, we present an update of the μbar CH_4 mixing ratios (Kim et al., 2014) of Jupiter by reanalyzing the ISO (Infrared Space Observatory) 3-μm spectrum (Fig. 1A) using vibrational-relaxation rates measured by Menard-Bourcin et al. (2005). The ISO aperture covered a large area including equatorial and temperate regions, and the derived mixing ratio curve should represent an average value of these regions. We find that our updated mixing ratio curve matches Model C of Moses et al. (2005) within the uncertainties (Fig. 1A), whereas the mixing curve of Kim et al. (2017) is only barely consistent with Model C. We note that the mixing ratio curves of equatorial regions derived from the New Horizon/occultation observations of Greathouse et al. (2010) are consistent with Model C. The error bars in our updated equatorial mixing ratio curves for the 8CNPHS (Fig. 1A) are smaller than those of the mixing ratios derived by Kim et al. (2017). Accordingly, we estimate that an increase in temperature greater than ~40 K at the μbar levels in the auroral regions is needed to produce an increase in the thermal emission at 3.3 μm that is comparable to the 1-σ uncertainty in Fig. 2. The synthetic spectra of the 3.3-μm CH_4 band presented in Fig. 1 are made from this updated mixing ratio curve and the temperature-pressure profile of a quiescent 8CNPHS in Fig. 3b of Kim et al. (2017).

We note, however, that the Model C mixing ratio curve lies an order of **magnitude** below the theoretical curve of the auroral region at 1 μbar of Wong et al. (2003; see their Fig. 1A), which is an update of Wong et al. (2000). An improved mixing ratio curve than that of Wong et al. (2003), based on an updated auroral chemistry, will be presented in a future study. Previously, the global CH_4 mixing ratios at the μbar levels, excluding the auroral regions, were thought to be uniform within ±20% across the planet (Drossart et al., 2001).

(4c) Auroral particle bombardment and Joule heating

A possible cause of the difference in the positions of the bright spots of CH_4 and C_2H_6 emission, in addition to the possibility of regional temperature differences, might be a difference in the vertical mixing ratios of the two hydrocarbons. This would expose the two species to precipitating auroral particles with different energies and/or vertically different Joule heating. Further investigations on the vertically-resolved spectro-images of the auroral regions observed by JIRAM are desirable to resolve this issue.

Kim et al. (2017) proposed a possible mechanism for the stationary nature and brightening of the 8CNPHS, that locally-fixed and transient but energetic auroral particle precipitations can warm the mbar pressure levels. The heat capacity at mbar altitudes is higher than at μbar altitudes. High temperatures at mbar altitudes can be maintained at least for several months (e.g., Zhang et al., 2013). Although we do not find an apparent correlation between the 3-μm emissions on the

8CNPHS and the solar activities, the short time interval during which these observations were made means that the mechanism proposed by Kim et al. (2017) has not been ruled out.

5) Conclusions

High-resolution 3.315-3.405 μm spectroscopy of Jupiter at 65° North latitude between March and July 2018 reveals that the highest emission intensities of CH_4 and C_2H_6 at the 8CNPHS and nearby longitudes, were 3 to 4 times greater than those of the lowest emissions, and also that the temperature of the 3-μm CH_4 emission at the 8CNPHS was relatively steady and much lower than at the 3CNPHS. The influence of low solar activity on the 8CNPHS is not quantitatively understood. During the same four-month period, there was lack of correlation between the 3-μm CH_4, C_2H_6, and H_3^+ emissions at the 8CNPHS and the solar wind characteristics such as dynamic pressure, densities, radial velocities, and temperatures. We also find no apparent correlation between the brightening of the 3-μm emissions on the 8CNPHS and the accumulations of solar wind particles during the quiescent intervals that Kita et al. (2016) claimed for the ultraviolet emissions of the auroral regions. We note, however, that the 2018 was only ~2 years before the next solar minimun around ~2020, and possibly close to the historic grand solar minimum, which has a ~100 year period. Since the 3-μm CH_4 and C_2H_6 emissions originate from the μbar pressure levels of the 8CNPHS, the lack of correlation indicates that the solar wind activities induced no significant changes in μbar level temperatures (<40K) and/or mixing ratios of these molecules at the μbar levels during the period. The lack of correlation is in contrast to the 8-μm result of Sinclair et al. (2019), who found that there is a coincidence between solar wind activity and 8-μm brightening of the 8CNPHS. However, the above upper limit on changes in μbar temperature does not conflict with Sinclair et al., who estimated that a significant 8-μm brightening of the 8CNPHS would occur with a 20K increase at μbar levels.

Acknowledgments

This paper is based in large part on observations obtained at the Gemini Observatory, which is operated by the Association of Universities for Research in Astronomy, Inc., under a cooperative agreement with the NSF on behalf of the Gemini partnership: the National Science Foundation (United States), National Research Council (Canada), CONICYT (Chile), Ministerio de Ciencia, Tecnología e Innovación Productiva (Argentina), Ministério da Ciência, Tecnologia e Inovação (Brazil), and Korea Astronomy and Space Science Institute (Republic of Korea). SJK acknowledges support from the Basic Science Research Program(2018R1D1A1B07046476), and the Brain Korea 21 Plus (BK21+) program through NRFfunded by the Ministry of Education, Science and Technology. SJK thanks a discussion with Prof. Gwang Son Choe regarding solar cycles, and useful information on collisional relaxation rates provided by Dr. Peter Panka. This research was supported by K-GMT Science Program (GN-2018A-Q-221) of Korea Astronomy and Space Science Institute. YLY acknowledges support by NASA New Frontiers Program. The solar wind data used in this study are available upon a request to C.Tao (chihiro.tao@nict.go.jp) and/or at AMDA database (http://amda.cdpp.eu). We thank the anonymous referees for their many detailed suggestions, which greatly improved

the content of this paper.

References

Altieri, F., Dinelli, B. M., Migliorini, A., Moriconi, M. L., Sindoni, G., Adriani, A., Mura, A., Fabiano, F., 2016, Mapping of hydrocarbons and H_3^+ emissions at Jupiter's north pole using Galileo/NIMS data. Geophys. Res. Lett., 43, 11,558–11,566. https://doi.org/10.1002/2016GL070787.

Baron, R. L., Owen, T.;, Connerney, J. E. P., Satoh, T., Harrington, J., 1996. Solar wind control of Jupiter's H_3^+ auroras. Icarus, 120, 437-442. https://doi.org/10.1006/icar.1996.0063

Caldwell, J., Tokunaga, A.T., Gillett, F.C., 1980. Possible infrared aurorae on Jupiter. Icarus, 41, 667-675. https://doi.org/10.1016/0019-1035(80)90135-9

Cowley, S. W. H., Bunce, E. J., 2001. Origin of the main auroral oval in Jupiter's coupled magnetosphere-ionosphere system. Planet. Space Sci. 49, 1067–1088. https://doi.org/10.1016/S0032-0633(00)00167-7

Drossart, P., Bézard, B., Atreya, S. K., Bishop, J. Waite Jr., J. H., Boice, D., 1993. Thermal profiles in the auroral regions of Jupiter. J. Geophys. Res. 98 (E10), 18,803-18,811. https://doi.org/10.1029/93JE01801

Drossart, P., Fouchet, T., Raynaud, E., Sicardy, B., Widemann, T., Waite, J. H., Gladstone, G. R., 2001. The upper atmosphere of Jupiter from VLT/ISAAC observations. Bull. Am. Astron. Soc. 33, 1026.

Greathouse, T.K. et al., 2010. New Horizons Alice ultraviolet observations of a stellar occultation by Jupiter's atmosphere. Icarus 208, 293–305. http://dx.doi.org/10.1016/j.icarus.2010.02.002.

Hill, T. W., 2004. Auroral structures at Jupiter and Earth. Adv. Space Res. 33, 2021–2031. https://doi.org/10.1016/j.asr.2003.05.037

Hill, T. W., 2001. The Jovian auroral oval. J. Geophys. Res. 106, 8101–8107. https://doi.org/10.1029/2000JA000302

Kim, S. J., Caldwell, J., Rivolo, A. R., Wagener, R., Orton, G. S., 1985. Infrared polar brightening on Jupiter. III. Spectrometry from the Voyager 1 IRIS experiment. Icarus 64, 233–248. https://doi.org/10.1016/0019-1035(85)90088-0

Kim, S.J., Geballe, T.R., Noll, K.S., 2000. Three-micrometer CH_4 line emission from Titan's high-altitude atmosphere. Icarus 147, 588–591. doi:10.1006/icar.2000.6481

Kim, S.J. et al., 2010. High-resolution 3-lm spectra of Jupiter: Latitudinal spectral variations influenced by molecules, clouds, and haze. Icarus 208, 837–849. http://dx.doi.org/10.1016/j.icarus.2010.03.024

Kim, S. J., Sim, C. K., Sohn, M. R., Moses, J. I., 2014. CH_4 mixing ratios at microbar pressure levels of Jupiter as constrained by 3-micron ISO data. Icarus 237, 42–51. https://doi.org/10.1016/j.icarus.2014.04.023

Kim, S. J., Sim, C. K., Ho, J. Geballe, T. R., Yung, Y. L., Miller, S. Kim, Y. H., 2015. Hot CH_4 in the polar regions of Jupiter, Icarus 257, 217–220. https://doi.org/10.1016/j.icarus.2015.05.008

Kim, S. J., Geballe, T. R., Greathouse, T., Yung, Y. L., Miller, S., Orton, G. S., Minh, Y. C., 2017. Temperatures and CH_4 mixing ratios near the homopause of the 8 μm north polar hot spot of Jupiter. Icarus 281, 281-285. https://doi.org/10.1016/j.icarus.2016.09.017

Kita, H., Kimura, T., Tao, C., Tsuchiya, F., Misawa, H., Sakanoi, T., Fujimoto, M., 2016. Characteristics of solar wind control on Jovian UV auroral activity deciphered by long-term Hisaki EXCEED observations: Evidence of

preconditioning of the magnetosphere? Geophys. Res. Lett. 43, 6790–6798. https://doi.org/10.1002/2016GL069481

Kostiuk, T., Livengood, T. A., Fast, K. E., Hewagama, T., Schmülling, F., Sonnabend, G., Delgado, J., 2011. Is there solar control of mid-infrared aurora on Jupiter? 2011. EPSC Abstracts 6, EPSC-DPS2011-1660

Menard-Bourcin, F., Boursier, C., Doyennette, L., Menard, J., 2005. Rotational and Vibrational Relaxation of Methane Excited to $2\nu_3$ in CH_4/H_2 and CH_4/He Mixtures at 296 and 193 K from Double-Resonance Measurements. J. Phys. Chem. 109, 3111-3119. https://doi.org/10.1021/jp0448649

Moses, J.I., Fouchet, T., Bezard, B., Gladstone, G.R., Lellouch, E., Feuchtgruber, H., 2005. Photochemistry and diffusion in Jupiter's stratosphere: Constraints from ISO observations and comparisons with other giant planets. J. Geophys. Res. 110, E08001. https://doi.org/10.1029/2005JE002411

Moriconi, M. L., Adriani, A., Dinelli, B. M, and 26 coauthors, 2017. Preliminary JIRAM results from Juno polar observations: 3. Evidence of diffuse methane presence in the Jupiter auroral regions. Geophys. Res. Lett. 44, 4641-4648. https://doi.org/10.1002/2017GL073592

Nichols, J. D., Bunce, E. J., Clarke, J. T., Cowley, S. W. H., Gérard, J.-C., Grodent, D., Pryor, W. R., 2007. Response of Jupiter's UV auroras to interplanetary conditions as observed by the Hubble Space Telescope during the Cassini flyby campaign. J. Geophys. Res. 112 (A2) A02203. https://doi.org/10.1029/2006JA012005

Nichols, J. D., Badman, S.V., Bagenal, F., and 24 cothors. 2017. Response of Jupiter's auroras to conditions in the interplanetary medium as measured by the Hubble Space Telescope and Juno. Geophys. Res. Lett. 44, 7643-7652. doi:10.1002/2017GL073029

Pryor, W. R., Stewart, A. I. F., Esposito, L. W., and 20 coauthors, 2005. Cassini UVIS observations of Jupiter's auroral variability. Icarus 178 (2), 312-326. https://doi.org/10.1016/j.icarus.2005.05.021

Sinclair, J. A., Orton, G. S., Greathouse, T. K., Fletcher, L. N., Moses, J. I., Hue, V., Irwin, P. G. J., 2018. Jupiter's auroral-related stratospheric heating and chemistry II: Analysis of IRTF-TEXES spectra measured in December 2014. Icarus 300, 305-326. https://doi.org/10.1016/j.icarus.2017.09.016

Sinclair, J. A., Orton, G. S., Fernandes, J., and 14 coauthors, 2019. A brightening of Jupiter's auroral 7.8-μm CH_4 emission during a solar-wind compression. Nature Astronomy, https://doi.org/10.1038/s41550-019-0743-x

Solanki, S.K., Krivova, N.A., 2011. Analyzing solar cycles. Science, 334, 916-917. DOI: 10.1126/science.1212555

Tao, C., Kataoka, R., Fukunishi, H., Takahashi, Y., Yokoyama, T., 2005. Magnetic field variations in the jovian magnetotail induced by solar wind dynamic pressure enhancements. J. Geophys. Res. 110 (A11), A11208. https://doi.org/10.1029/2004JA010959

Thatcher, L. J., Müller, H.-R., 2011. Statistical investigation of hourly OMNI solar wind data. J. Geophys. Res. 116 (A12), A12107. https://doi.org/10.1029/2011JA017027

Waite, J. H., Gladstone, G. R., Lewis, W. S., Goldstein, R., McComas, D. J., Riley, P., Walker, R. J., Robertson, P., Desai, S., Clarke, J. T., Young, D. T., 2001. An auroral flare at Jupiter. Nature 410 (6830), 787-789. https://doi.org/10.1038/35071018

Wong, A.-S., Lee, A. Y. T., Yung, Y. L., Ajello, J. M., 2000. Jupiter: Aerosol Chemistry in the Polar Atmosphere.

Astrophys. J. 534 (2), L215-L217. https://doi.org/10.1086/312675

Wong, A.-S., Yung, Y. L., Friedson, A. J., 2003. Benzene and Haze Formation in the Polar Atmosphere of Jupiter. Geophys. Res. Lett. 30 (8), 1447. http://doi.org/10.1029/2002GL016661

Yates, J.N., Achilleos, N., Guio, P., 2014. Response of the Jovian thermosphere to a transient 'pulse' in solar wind pressure, Planet. Space Sci. 91, 27-44. https://doi.org/10.1016/j.pss.2013.11.009

Zhang, X., Nixon, C.A., Shia, R.L., West, R.A., Irwin, P.G., Yelle, R.V., Allen, M.A., Y.L. Yung, Y.L., 2013. Radiative Forcing of the Stratosphere of Jupiter, Part I: Atmospheric Cooling Rates from Voyager to Cassini, Planetary and Space Science, 88, 3-25. http://dx.doi.org/10.1016/j.pss.2013.07.0035

Figure Captions

Fig. 1abcd. Four GNIRS spectra (thick black traces) of the jovian 8CNPHS and telluric standard stars (dashed lines) observed at 3.33-3.36 μm between March and July 2018. Each the four spectra is the sum of the spectra of ~100 rows of the GNIRS detector array within **+/-2.5** arcseconds of the center of the 8CNPHS at 180° (SysIII) longitude as shown in Fig. 2. The gaps in the jovian spectra correspond to regions of low telluric transmission at the wavelengths of CH_4 and H_2O lines. Three strong telluric absorption by CH_4 P-branch lines are indicated by thick blue bars. Blue and violet traces are CH_4 model spectra with rotational temperatures as shown; green traces denote H_3^+ lines. The estimated $\pm 1\sigma$ uncertainty at wavelengths where the atmospheric transmission is at least 80%, and the wavelength interval containing blended CH_4 Q combination band lines, are both shown at the left edges of the panels. Wavelengths of C_2H_6 ν_7 lines are denoted by vertical black lines. The vertical scale is expanded in order to reveal weak lines, resulting in truncation of some of the strong jovian emission lines; e.g., at 3.345 μm.

Fig. 2. East-west relative intensity profiles for the March-July observations of CH_4, C_2H_6, and H_3^+ emission lines. The data used to produce the CH_4 profile are the intensities of weak and blended Q lines between 3.330 and 3.336 μm excluding the vicinities of the CH_4 P(2) and C_2H_6 ν_7 lines. The horizontal axis is in arcsec for the May 14 data only; and the other profiles are adjusted to the same longitudinal scale as that of the May 14 data. The extent of the 8-μm CH_4 north polar hot spot (8CNPHS) is denoted by the horizontal line in the top panel. The intensity profiles in each panel are relative to the profile containing the highest peak, and are scaled so that the peak intensity is 30 units.

Fig. 3. Comparisons of the 3.3-μm CH_4, C_2H_6, and H_3^+ emission intensities within the 8CNPHS and the solar wind dynamical pressures (nPa), from the solar-wind propagation model of Tao et al. (2005). The highest CH_4, C_2H_6, and H_3^+ intensities are set to be 0.6 of the vertical scale of each panel. Error bars of ± 2 days based on the model uncertainty at the orbit of Jupiter are shown along with the intensity error bars.

Fig. A1. Mixing ratio ranges of CH_4 for two curves (red), which correspond to the $\pm 1\sigma$ error bars of the relaxation rate of Menard-Bourcin et al. (2005). Also presented are two theoretical mixing ratio curves of CH_4 for the auroral regions

(Wong et al., 2000; 2003), and theoretical Model C (Moses et al., 2005) and Model D (Kim et al., 2014) for non-auroral regions.

(Appendix A) CH_4 Mixing Ratios Near μbar-Pressure Levels

Kim et al. (2014) derived the μbar CH_4 mixing ratio in the equatorial and temperate zones of Jupiter from an analysis of the 3.3-μm CH_4 emission spectrum observed by the Infrared Space Observatory (ISO). The large uncertainies in the derived ratio (see Fig. 4 of Kim et al., 2014) resulted from the large uncertainties in the vibrational relaxation rates for the 3-μm CH_4 transitions due to the lack of reliable laboratory measurements at low temperatures, especially at Jupiter's temperatures. Here we recalculate the μbar CH_4 mixing ratio, adopting the vibrational relaxation rate of $2.8 \pm 0.8 \times 10^{-12}$ cm^3 sec^{-1} $molecule^{-1}$ by collisions with H_2 at 193 K measured by Menard-Bourcin et al. (2005). In Fig. A1, we present the derived mixing ratio, displaying two curves which correspond to the ±1σ error bars of the relaxation rate.

The measured rate of Menard-Bourcin et al. (2005) at 193 K is somewhat unusual, because it is greater than the room temperature (296K) value of $2.45 \pm 0.92 \times 10^{-12}$ cm^3 sec^{-1} $molecule^{-1}$ measured by the same authors. This lower rate at a higher temperature conflicts with the value predicted by elementary kinetic theory, in which the rate is proportional to the square root of temperature. However, the uncertainties in both measured rates presented by those authors are too large to definitely determine the direction of the temperature dependency. Previously, Hess and Moore (1976) measured a rate of 2.6×10^{-12} cm^3 sec^{-1} $molecule^{-1}$ at 295 K, which is also consistent with the rates measured by Menard-Bourcin et al. (2005). Our previous work (Kim et al., 2017), using the room temperature value of Hess and Moore (1976) and extrapolating to Jupiter's temperatures by adopting the elementary kinetic theory, should be valid considering the relatively large uncertainties in the measured rate of Menard-Bourcin et al. (2005).

Highlights

- Gemini /GNIRS 3.3 - 3.4 μm spectra of the 8-μm CH_4 north polar hot spot (8CNPHS) of Jupiter were obtained.
- Four occasions during a five-month period in 2018 were observed.
- The variability of the 3-μm emission intensities of CH_4, C_2H_6, and H_3^+ was studied.
- The peak intensities of these species showed the highest 3-4 times greater than the lowest.
- We find lack of correlation between the 3-μm hydrocarbon intensities at the 8CNPHS and the solar wind strength.

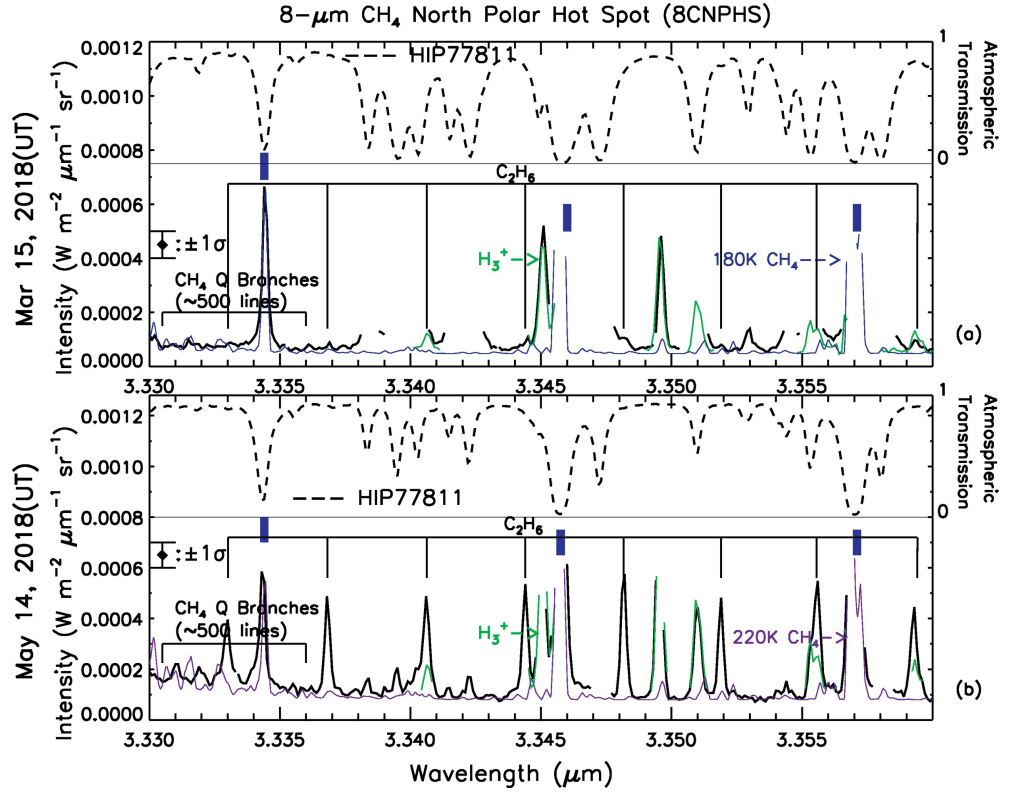
8−μm CH4 North Polar Hot Spot (8CNPHS)
HIP77811
C2H6
H3+
CH4 Q Branches (~500 lines)
±1σ
180K CH4
220K CH4
Atmospheric Transmission
Intensity (W m−2 μm−1 sr−1)
Mar 15, 2018(UT)
May 14, 2018(UT)
(a)
(b)
Wavelength (μm)

Figure 1ab

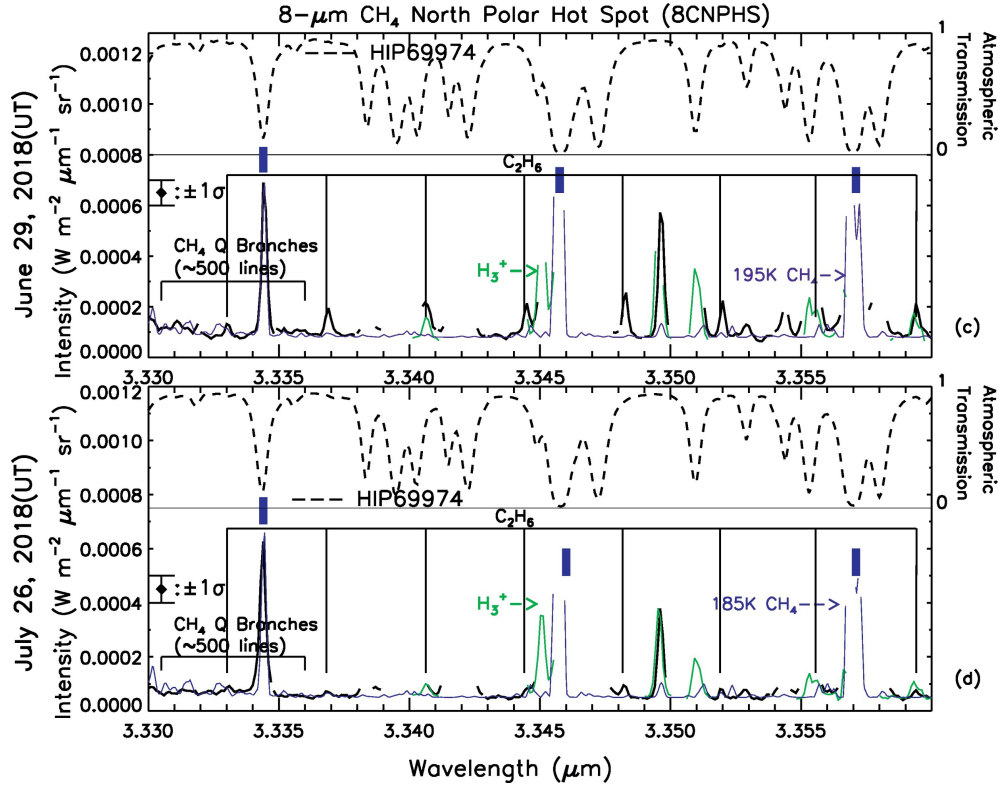
8−μm CH4 North Polar Hot Spot (8CNPHS)
HIP69974
Atmospheric Transmission
June 29, 2018(UT)
Intensity (W m−2 μm−1 sr−1)
C2H6
±1σ
CH4 Q Branches (~500 lines)
H3+
195K CH4
(c)
July 26, 2018(UT)
185K CH4
(d)
Wavelength (μm)

Figure 1cd

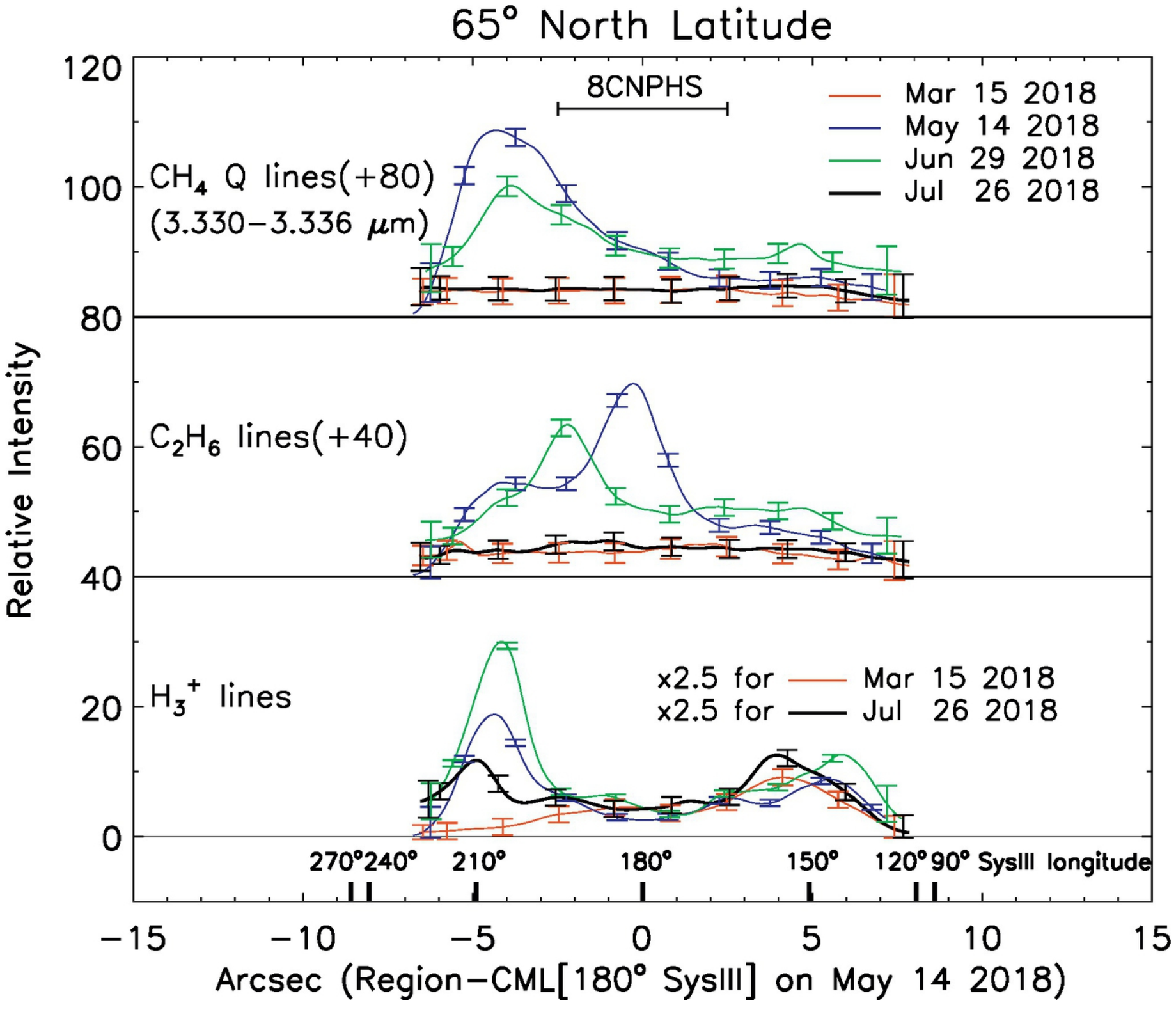
65° North Latitude
8CNPHS
Mar 15 2018
May 14 2018
Jun 29 2018
Jul 26 2018
CH4 Q lines(+80)
(3.330–3.336 μm)
C2H6 lines(+40)
H3+ lines
x2.5 for Mar 15 2018
x2.5 for Jul 26 2018
Relative Intensity
120
100
80
60
40
20
0
270° 240° 210° 180° 150° 120° 90° SysIII longitude
−15 −10 −5 0 5 10 15
Arcsec (Region−CML[180° SysIII] on May 14 2018)

Figure 2

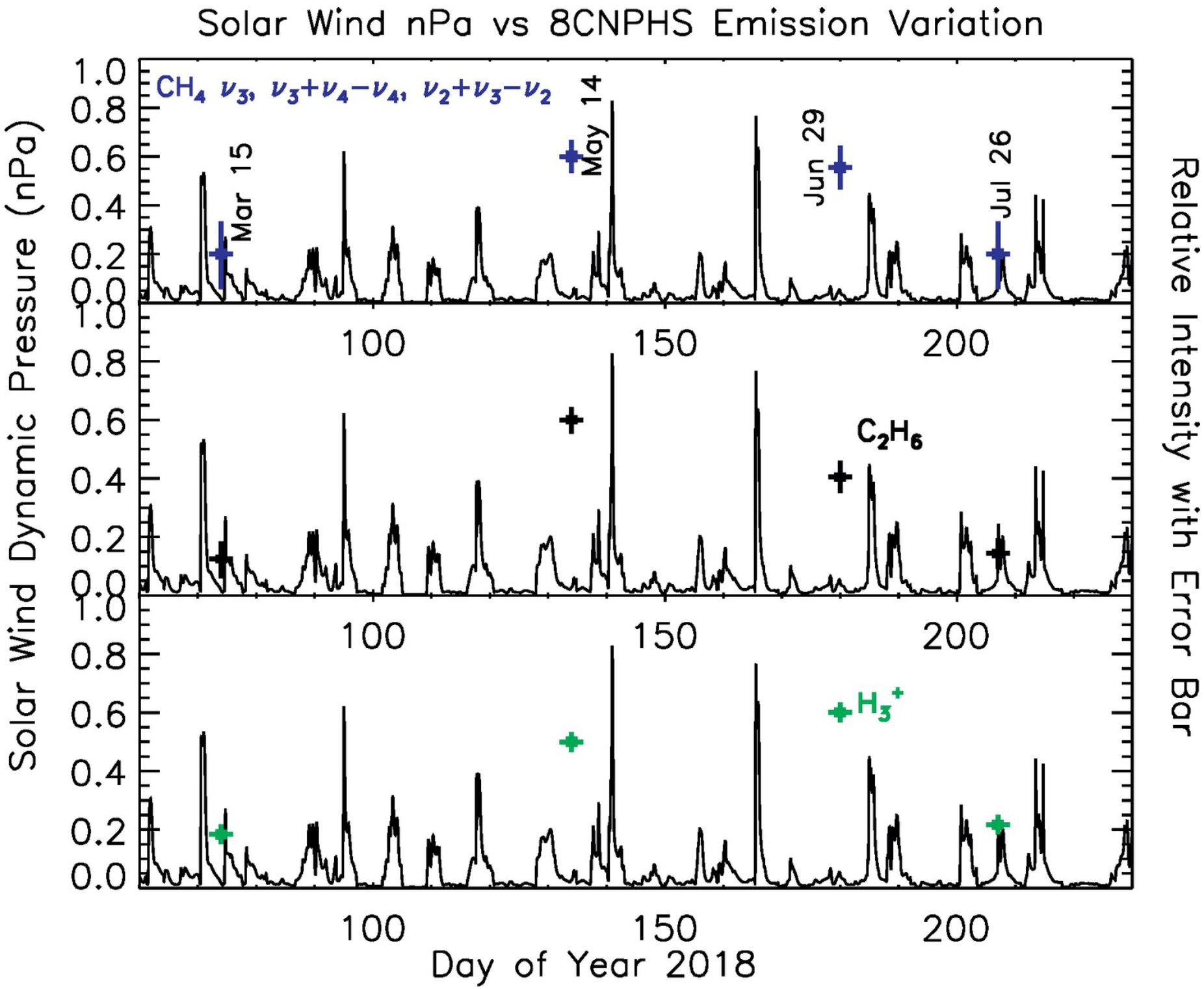
Solar Wind nPa vs 8CNPHS Emission Variation
CH4 ν3, ν3+ν4−ν4, ν2+ν3−ν2
Mar 15
May 14
Jun 29
Jul 26
C2H6
H3+
Solar Wind Dynamic Pressure (nPa)
Relative Intensity with Error Bar
Day of Year 2018
0.0
0.2
0.4
0.6
0.8
1.0
100
150
200

Figure 3